

In-situ Fourier Transform InfraRed Spectroscopy as a Probe of the Electrode/Electrolyte Interface

P. A. Christensen

Department of Chemistry, Bedson Building, The University, Newcastle upon Tyne, NE1 7RU UK

1. Introduction

Over the last two decades FTIR spectroscopy has become an established *in-situ* analytical tool for the study of mechanism at the electrode/electrolyte interface[1][2], and the aim of this presentation is to illustrate the power and the practical aspects of the technique using examples of work carried out in Newcastle. The chosen examples are:

- (1) The potential-induced change in orientation of thiopyridine at a gold electrode[3]. This aspect of the paper illustrates the power and sensitivity of the technique with respect to the study of potential-induced changes in orientation of adsorbed organic monolayers. Prior to this work, it was generally accepted that the sensitivity demanded by such studies required sophisticated data collection techniques such as lock-in detection. However, the change in orientation of thiopyridine, (one of the first organics capable of promoting enzyme electrochemistry as a monolayer), was followed using straightforward data collection and over a reasonably short data collection time.
- (2) Ru(Bipy)₃²⁺/Nafion films have attracted attention over a number of years[see, for example, 4 - 10, and references therein] as a result of their potential application in systems such as molecular photoelectric devices. Nafion films containing redox species can, in principle, be fabricated in two entirely different ways: in the first approach, the redox complex is added to a Nafion sol, and the resultant mixture allowed to evaporate to form an *Incorporated* film, referred to below as a Type (I) film. The second method of fabrication employs ion exchange into pre-formed Nafion films, a process necessarily restricted to cationic redox species; such films are referred to below as Type (A) *Absorbed* films. Despite the extensive literature on the Ru(Bipy)₃²⁺/Nafion system, a number of aspects remain under discussion:
 - (1) The mechanism responsible for the turnover of the Ru(III) complex during oxidation.
 - (2) Whether the inactive form of the complex in type (I) films remains so as the films are increasingly loaded with the complex.
 - (3) The reason for the substantive differences in behaviour of type (I) and type (A) films in terms of their kinetic and spectrophotometric responses.

Space does not allow a full treatment of this system, so the discussion below will focus firstly on the IR response observed on oxidising the Ru(II) species in the Nafion, and then will concentrate on problem (1); a full treatment may be found elsewhere [11].

- (3) The mechanism of the photoelectrochemical oxidation of methanol at thermal TiO₂ films as a function of temperature between 10 °C and 50 °C. In addition to making *in-situ* FTIR very much more quantitative, the future of the technique must lie in extending its application on the time, length and temperature scales. Following the work of Osawa[12], we are developing an *in-situ* FTIR system capable of studying reversible electrochemical processes on the *c.* μs timescale. The chosen example, however, illustrates two aspects of our current capability: the ability to study semiconductor surfaces *in-situ* whilst under irradiation, and the ability to study electrochemical reactions *in-situ* as a function of temperature; currently, the system has been tested over the range -10 °C to +70 °C.

The first *in-situ* IR study of a photoexcited electrode was reported by Bockris and co-workers [13] and concerned the reduction of CO₂ at p-CdTe, whilst Peter and co-workers reported IR studies on the photocorrosion of n-Si[14]. More recently, Christensen *et al.* [15] studied the photoelectrochemical oxidation of ethylene glycol and formate at (001) Rutile, and Kavan and co-workers[16] employed *in-situ* FTIR to elucidate the mechanism of solvent breakdown at irradiated Anatase TiO₂ electrodes in propylene carbonate and acetonitrile.

The work reported in this paper extends our mechanistic studies of photodegradation on semiconducting TiO₂ electrodes into the temperature domain, and reports a study of a thermally-formed TiO₂ film under irradiation and electrochemical control at 10 °C and 50 °C in aqueous perchlorate, in the absence and presence of 1M methanol. This work is part of our ongoing research effort on the photoelectrochemical detoxification and disinfection of water [15][17 - 22], which recently included an assessment of the activities of a range of TiO₂ - based electrodes towards the oxidation of organics and killing of *Cryptosporidium parvum*[22]. Thus, studies in this and other laboratories have established that the surface chemistry on TiO₂ electrodes is a sensitive function of morphology, surface area, preparation method and crystalline form[21][22][23 - 26]. In our hands, thermal TiO₂ films, (although largely amorphous), have proved effective at mineralising a number of organics, and the aim of this paper was to investigate the nature of the mechanisms of such transformations, using methanol as a model organic, and how these mechanisms change with temperature

2. Experimental

Details of the chemicals used and all experimental procedures may be found in the relevant papers[3][11][27][28]. Briefly:

The IR reflective working electrode (Au, Basal Plane Graphite, [BPG], Pt or thermal Ti/TiO₂ film) was cut in the shape of a 'top hat' to expose 0.64 cm² to the electrolyte. Contact to the electrode was maintained *via* a screw and pushrod mechanism (BPG, Au and Pt electrodes), or *via* a wire mounted on the rear of the electrode (TiO₂ electrode). The counter electrode was a 1 cm x 2 cm Pt gauze or Pt wire, and the reference was an Ag/AgCl electrode (Sentek) or SCE (S. H. Scientific). The window was a 25 mm *dia.* 3mm thick CaF₂ plate. The cell employed in the variable-

temperature experiments was modified to include a water jacket, with the temperature of the TiO₂ electrode monitored *via* a standard thermocouple (RS Components). The TiO₂ electrode was irradiated with UV light (150W Xe lamp) *in-situ* *via* a 1m flexible liquid light guide (Oriel). The working electrode was re-positioned against the window after each change in temperature, to prevent the optical alignment deteriorating due to thermal drift.

The FTIR spectrometer was either a Bio-Rad FTS-40 or a Bio Rad FTS-60, with narrow band liquid nitrogen-cooled MCT detectors. The potential of the working electrode was controlled by an Atari-based Oxsys Micros Electrochemical Interface, OEI, which also controlled the FTIR spectrometer.

The formation of adsorbed thiopyridine was achieved by immersing the gold electrode into an aqueous 1mM solution of 4,4'-dithiopyridine for 10 minutes, followed by thorough washing with water.

Ru(bipy)₃²⁺/Nafion films were formed as follows: the 5% Nafion solution was diluted with ethanol to form a 2% solution. The films were then formed either: (i) by dropping 5μL of the 2% Nafion solution onto the electrode (Pt or BPG), allowing the film to dry, and then immersing the coated electrode in aqueous Ru(bipy)₃Cl₂, [Type(A)-film], or (ii) by making up a solution of the required concentration of Ru(bipy)₃Cl₂ in the Nafion solution, dropping 5μL of the solution onto the electrode and allowing the film to dry, [Type (I) film]. On the basis of simple calculations based upon the density of the Nafion, these procedures result in films 0.5 - 1 μm in thickness. On the basis of the known concentration of Ru(bipy)₃²⁺ in the solution, the *amount* of the latter in the Type (I) film is 2×10^{-8} moles for a Type (I) film derived from a 4 mM solution.

The data are presented as plots of $\Delta R/R = (S_s - S_{ref})/S_{ref}$ or $\log_{10}[S_s / S_{ref}]$, "Absorbance", vs cm^{-1} , where S_s is a spectrum, (8 cm^{-1} resolution, 100 co-added and averaged scans, unless otherwise stated), taken at a particular potential or time after the reference spectrum S_{ref} was taken. Since $\log_{10}[S_s/S_{ref}] = \log_{10}[S_s] - \log_{10}[S_{ref}]$, both data manipulations effectively results in difference spectra, where peaks pointing up, to +Abs or + $\Delta R/R$, represents the *loss* of absorbing species at S_s vs S_{ref} , and peaks pointing down, to -Abs or - $\Delta R/R$, are attributable to the *gain* of absorbing species. This convention was chosen to conform with our previous work in *in-situ* FTIR.

3. Results and Discussion

3.1 The potential-dependent reorientation of adsorbed thiopyridine at a gold electrode

Hill[29] has shown that that 4,4'-dithiopyridine, SSbipy, promotes electron transfer between an electrode and cytochrome *c* at pH 7 in phosphate buffer. SERS and ellipsometric studies have shown that the promoter dissociatively adsorbs at a Au electrode[30][31] from its solution in water to give the thiopyridine fragment, but the

adsorbate shows no electrochemistry over the potential range at which the redox chemistry of cytochrome *c* is observed. Until our work[3], the potential dependence of the orientation of the adsorbed thiopyridine had not been reported.

Fig. 1 shows typical spectra taken using both s- and p- polarized light (*via* a KRS-5 polarizer) of the coated gold electrode in pH 7.1 phosphate buffer/0.1M NaClO₄; note the scale on the *y*-axis, and the signal/noise ratio. The spectra were collected at the end of an experiment in which the potential was stepped up from -0.2 V to +0.3V vs SCE in 100 mV increments, with spectra being collected at each step (750 [p-polarized experiments] or 500 [s-polarised experiments] co-added and averaged scans per scanset, 8 cm^{-1} resolution) and normalised to the reference collected at 0.2V. As may be seen from the fig. 1, two loss features, near 1615 cm^{-1} and 1485 cm^{-1} , and a single gain feature, near 1580 cm^{-1} , were observed, whose intensities increased as ΔV^2 up to 0.2V. These bands were only observed using the p-polarized light, a clear indication of the operation of the surface selection rule[32], confirming that the process taking place is one confined to the surface. Below 1400 cm^{-1} , the spectra were obscured by a relatively intense ($c. 5 \times 10^{-3} \Delta R/R$) due to the movement of ClO₄⁻.

As may be seen from fig. 2, the thiopyridine adsorbate is electro-inactive over the potential range studied, suggesting that the promoter is undergoing a potential-dependent change in orientation; stepping back down from 0.3V simply caused the bands in fig. 1 to change sign, clearly showing that the orientation change is reversible. By reference to the ring modes of pyridine[33] and the surface selection rule, it was possible to assign the 1615 cm^{-1} and 1485 cm^{-1} bands to the 8a and 19a vibrational modes of the molecule, and the 1580 cm^{-1} feature to the 8b mode, with the molecule tilting, from the vertical, edge-on towards the surface as the potential was increased, (see fig. 3). This was supported by the observed ΔV^2 dependence, which was predicted on the basis of simple dipole-moment considerations.

Figure 1 clearly shows the very high sensitivity possible using *in-situ* FTIR, despite the extremely simple data collection protocols that are generally employed.

3.2 Charge transport in tris(2, 2' bipyridine)Ru(II)/Nafion films

The electrochemistry of both types of film, type (I) and type (A) is typified in fig. 4, which shows the cyclic voltammograms of a 0.64 cm^2 Pt electrode (a) in a solution of 1 mM Ru(bipy)₃²⁺ in a background electrolyte of acidified 0.2M K₂SO₄ (pH 2); (b) covered with a film of Type (I) in the same background electrolyte; and (c) covered with a film of Type (A) (derived by immersion of the Nafion film in 1mM Ru(bipy)₃²⁺ solution for 15 min) in the same background electrolyte. These CV's were obtained at 5 mVs^{-1} , and are broadly similar in shape, with oxidation waves beginning near 1.1 V vs Ag/AgCl and peaks shifted slightly positive for Ru(bipy)₃²⁺ in the Type (I) film as compared to free solution or Type (A) films.

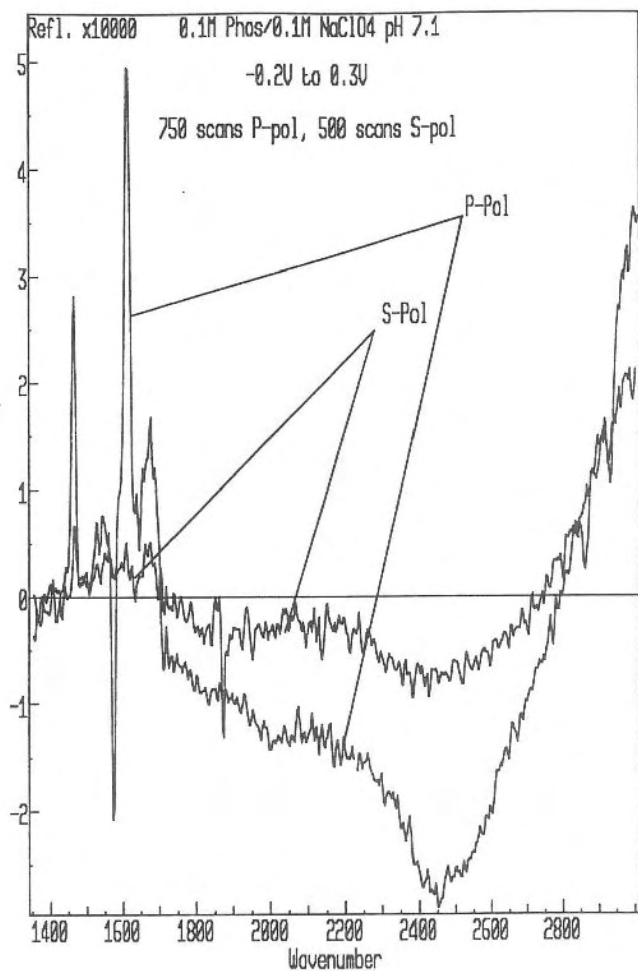


Fig. 1 Reflectance spectra, (8 cm^{-1} resolution, 500 [s-polarised] or 750 [p-polarised] co-added and averaged scans, of SSbipy adsorbed at a gold electrode immersed in N_2 -saturated pH 7.1 0.1M NaClO_4 /phosphate buffer. The spectra were collected at 0.3 V vs SCE and normalised to the reference spectrum taken at -0.2 V , using p-polarised and s-polarised light, as indicated on the figure. The second Pt counter electrode, held immediately behind the reflective working electrode, was poised at -0.3 V vs SCE throughout the IR data collection to reduce adventitious- O_2 , and so prevent the generation of $\cdot\text{OOH}$ obscuring the spectra.

Adsorbed thiopyridine on Au in pH 7 Phosphate buffer /0.1M NaClO_4

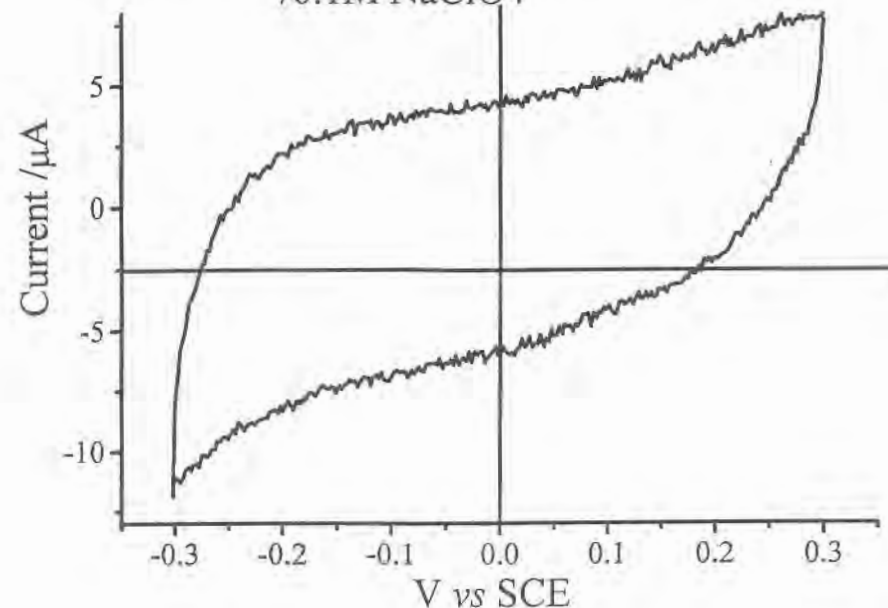


Fig. 2 Cyclic voltammogram of the electrode and solution in fig. 1. Scan rate 100 mV s^{-1}

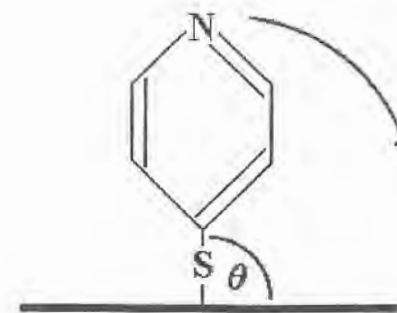


Fig. 3 The potential-dependent change in orientation of the adsorbed thiopyridine fragment observed on stepping the potential up from -0.2 V , see text for details.

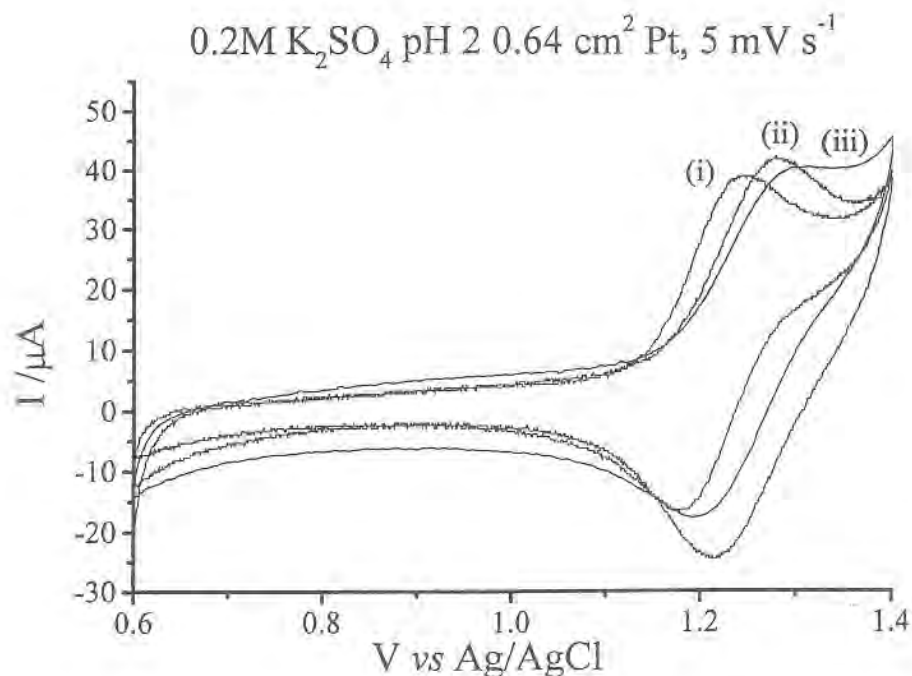


Fig. 4 Cyclic voltammograms of (i) 1mM Ru(bipy)₃²⁺, (ii) an adsorbed film [Type (A), 15 min.] and (iii) an incorporated [Type (I)] film (4mM Ru(bipy)₃²⁺), all at a 0.64 cm² Pt electrode, Electrolyte pH 2 0.2M K₂SO₄, scan rate 5 mV/s.

3.2.1 The IR Response observed on oxidation of the Ru(Bipy)₃²⁺ species in the Nafion

Figure 5 shows a comparison of the *in situ* FTIR spectra of the three systems in fig. 4, represented as difference spectra between potentials of 0.8 V vs SSCE (Silver-silver chloride reference electrode) where the Ru(bipy)₃²⁺ is essentially completely reduced, and 1.2 V where oxidation of the complex is expected to be close to completion. The spectrum taken in the 5 mM Ru(bipy)₃²⁺ solution has been increased by a factor of c. 50 for clarity. In each case, the spectra were collected at the end of a single potential step experiment from 0.7V and normalised to the reference spectrum of the Ru(II) state; 8 cm⁻¹ resolution and (a) 1000 co-added and averaged scans, (b) & (c) 100 co-added and averaged scans. The first point to emphasise with these data is the much lower changes in optical absorption associated with the Ru(bipy)₃²⁺ in solution. This arises because the data of fig. 5 is obtained using a thin-layer cell: direct calculation (see Experimental section) shows that the total amount of Ru(bipy)₃²⁺ in a Type (I)

film fabricated using 4 mM Ru(bipy)₃²⁺ solution is 2×10^{-8} moles, whereas the amount of Ru(bipy)₃²⁺ in a solution layer of thickness $\sim 1 \mu\text{m}$, *ie.* typical of that expected when using aqueous electrolyte[1], is $\sim 3.2 \times 10^{-10}$ moles; the factor of 60 between these two quantities corresponds very closely to the factor of 50 difference in intensities observed between the solution and Type (I) film FTIR data of fig. 5, taking the 1450 cm⁻¹ gain feature as our point of measurement (see Table 1). The change in IR absorption of the Type (A) film is very similar in magnitude to the Type (I) film, and the spectra for these two films show little difference.

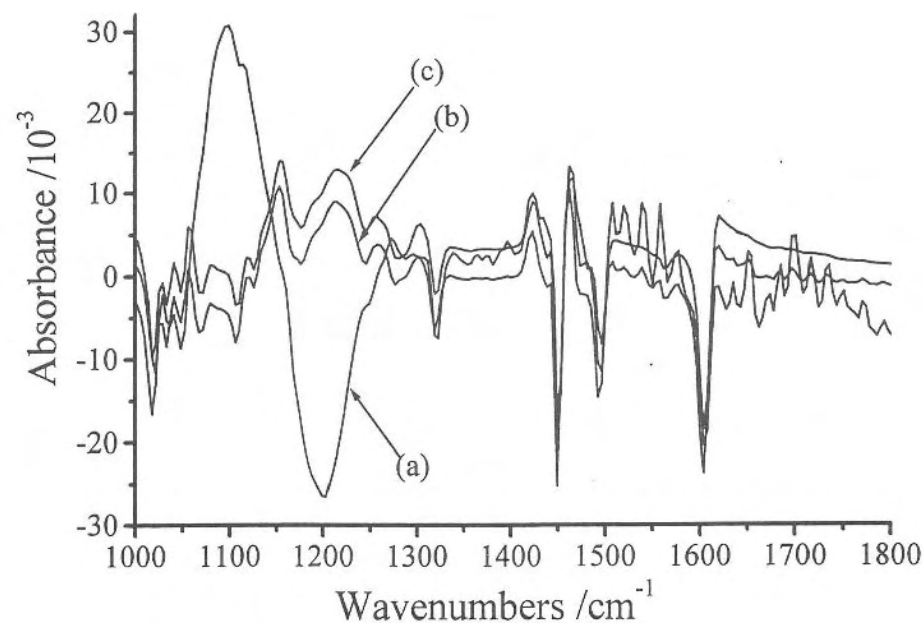


Fig. 5 *In-situ* FTIR spectra collected at 1.2V vs Ag/AgCl under similar conditions to those in figure 2: (a) 5mM Ru(bipy)₃²⁺ at a Pt electrode, spectrum has been scaled up by a factor of *ca.* 50, (b) the Type (I) film on BPG and (c) a Type (A) film (derived from immersion of Nafion in 5 mM Ru(bipy)₃²⁺ solution for 15 minutes) on BPG. In each case, the spectra were collected at the end of a potential step experiment from 0.7V and normalised to the reference spectrum of the Ru(II) state; 8 cm⁻¹ resolution and (a) 1000 co-added and averaged scans, (b) & (c) 100 co-added and averaged scans.

System	Cumulative Charge Passed /mC	Gain in absorbance of 1450 cm ⁻¹ band/10 ⁻³
5mM aq. Ru(bipy) ₃ ²⁺	1.1	0.4
Type (I) film	7.5	24
Type (A) film	10.6	25

Table 1 Cumulative charge passed, and the intensities of the 1450 cm⁻¹ gain feature, obtained during the experiments depicted in fig. 5.

Turning now to the details of the IR response, the gain and loss features seen are listed in Table 2, along with the literature assignments[34 - 36]; the loss features attributed to Ru(Bipy)₃²⁺ tracked exactly the gain features due to Ru(Bipy)₃³⁺. The IR spectrum of Ru(bipy)₃²⁺ has been analysed in terms of a C_{2v} model of a single Ru(bipy) unit[36]. This is obviously approximate, but all the IR bands found experimentally can be assigned to either A₁ or B₂ modes in this symmetry, with the former generally being less intense than the latter, so the IR spectrum of Ru(bipy)₃²⁺ is dominated by these B₂ modes, and the loss of these can clearly be seen in fig. 5. The only reasonably intense A₁ band clearly seen in the IR spectrum of Ru(bipy)₃²⁺ is at 1446 cm⁻¹; in fact, fig. 5 shows a strong gain at this frequency on stepping to positive potentials, and this and other gain peaks must correspond to Ru(bipy)₃³⁺, and specifically to the A₁ bands of this complex, as discussed below.

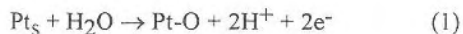
Unfortunately, there have been few reports of the IR spectrum of Ru(bipy)₃³⁺, with the most recent that has appeared[36] indicating relatively little change in the frequencies of the main skeletal vibrations as compared to Ru(bipy)₃²⁺. This is surprising, since back d_π - π* bonding in the latter would be expected to lower the bond order of the bipy framework and decrease the vibrational frequencies as compared to the oxidised form. The literature peaks for Ru(bipy)₃³⁺ are shown in Table 2 and, in brackets, other A₁ modes of Ru(bipy)₃²⁺ which are weak in the latter and expected to be much stronger in the former. This suggests that in the mid-IR

Gain Features /cm ⁻¹	Lit. values for A ₁ modes of Ru(bipy) ₃ ³⁺ [34] or sulphonate modes[35]	Loss Features /cm ⁻¹	Lit. values for B ₂ modes of Ru(bipy) ₃ ²⁺ [36] or sulphonate modes[35]
1605	1602	1466	1462
1564	(1563)	1425	1420
1497	1496	1306	1310
1450	1440	1158	1160
1320	(1320)		
		1153	-SO ₃ ⁻
1111		1224	-SO ₃ ⁻
1019		1060	-SO ₃ ⁻
1600-3000	-SO ₃ H		

Table 2. The IR bands observed during the oxidation of Ru(Bipy)₃²⁺ immobilised in Nafion using both Type (I) and Type (A) films, see fig. 5.

region, the spectrum of Ru(bipy)₃³⁺ is dominated by the A₁ bands, and this marked increase in the absorption cross-section of the A₁ modes in Ru(bipy)₃³⁺ can be understood by considering the change in geometry of the complex on vibrational excitation: increasing the bond length in the bipy framework will increase the energy of the bonding levels and decrease the energy of the π* levels, leading to increased σ-donation to the metal and increased d_π → π* donation to the ligand. The nett effect will be to change the ligand metal dipole of Ru(bipy)₃²⁺ very little and to lead, therefore, to a low absorption cross-section. By contrast, for Ru(bipy)₃³⁺, there is very little d_π → π* donation, and increasing the bond-length of the ligand skeleton will give rise to substantial changes in dipole moment. The reason why the B₁ modes are apparently 'switched off' remains unclear.

The region below 1300 cm^{-1} in the spectra of solution phase $\text{Ru}(\text{bipy})_3^{2+}$ is dominated by a broad gain feature near 1200 cm^{-1} and a broad loss feature near 1100 cm^{-1} . Interestingly, these features are also present if a pristine Nafion film is used with no $\text{Ru}(\text{bipy})_3^{2+}$ present in either film or solution. Simply stepping a Nafion-covered Pt electrode from 0.8 to 1.2 V shows bands in these two positions, and the gain and loss may be unambiguously assigned to HSO_4^- and SO_4^{2-} respectively outside the film, in the electrolyte[37]. This process is initiated by the formation of H^+ in solution arising from:



The protons diffuse out of the Nafion, decreasing the pH in the thin layer of the Infra-red cell. An elementary calculation shows that for the thin layer cells employed ($\sim 1\text{ }\mu\text{m}$ thick), even the monolayer reaction (1) can increase the local H^+ concentration in the thin layer towards 0.1 M, enough to protonate sulphate ions, at least partially. The very poor lateral diffusion ensures that this concentration is not transient on our timescales.

When $\text{Ru}(\text{bipy})_3^{2+}$ is present in the Nafion, whether of Type (I) or (A), this sulphate/bisulphate absorption change is *not* observed; instead, three strong loss features are observed, near 1224 cm^{-1} , 1153 cm^{-1} 1060 cm^{-1} . These bands are observed in the single-beam spectrum of Nafion, and may be attributed [35] to loss of $-\text{SO}_3^-$.

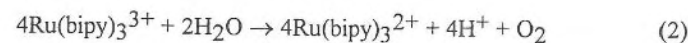
Concomitantly, there is a broad gain from 1600 to 3000 cm^{-1} , which may be assigned to the protonated $-\text{SO}_3\text{H}$ form. This suggests a substantial increase in pH locally *in the film*: the origin of the protons is now primarily the reduction of $\text{Ru}(\text{Bipy})_3^{3+}$ rather than Pt-O formation and evidently the film acts as a buffer. The most likely explanation is that regardless of the mode of incorporation of $\text{Ru}(\text{bipy})_3^{2+}$ in the film, on standing the Nafion film in the K_2SO_4 solution, cation exchange can take place with the incorporation of K^+ ions in the place of protons. This process is evidently facilitated by the $\text{Ru}(\text{bipy})_3^{2+}$ already present in the film, since in the pristine film, clear conversion of solution sulphate to bisulphate is seen. Generation of protons in the $\text{Ru}(\text{bipy})_3^{2+}$ /Nafion film then reverses this procedure, with expulsion of K^+ . That the local concentration of protons can rise to a high value in the film is evident from Table 1: a charge of 7.5 mC corresponds to a proton concentration of $\sim 1\text{ M}$ in a film of thickness $1\text{ }\mu\text{m}$.

3.2.2 The steady state current

Returning to problem (1) above; if the cumulative charges passed during the time-dependent spectroscopic experiments (which last for ~ 30 min) for the three different systems represented by fig. 5 are measured, the results are very surprising, as shown by the typical data in Table 3. For the Type (I) film, it can be seen that the total charge passed, 7.5 mC, greatly exceeds that expected on the basis of the total amount of $\text{Ru}(\text{bipy})_3^{2+}$ in the film (2×10^{-8} moles, see section 2.3), which would, on the basis of

a one-electron process, yield at most 2 mC. This can be seen more clearly in figs. 6(a) and (b) which show (a) the intensity of the 1450 cm^{-1} $\text{Ru}(\text{Bipy})_3^{3+}$ feature as a function of time measured during a potential step from 0.7V to 1.2V, and (b) the corresponding cumulative charge. Despite the fact that the change in the IR response is largely complete by $t = 15$ minutes, the charge data clearly show the existence of a steady-state current which continues irrespective of the IR response. This steady-state current was typically $1 - 4\text{ }\mu\text{A}$.

The only logical explanation for the charge and IR data is that some redox process is taking place to convert the oxidised $\text{Ru}(\text{bipy})_3^{3+}$ back to the Ru(II) complex; this is supported by experiments in which films switched to 1.2 V, held until steady-state is established, and then switched to open-circuit show a loss of $\text{Ru}(\text{bipy})_3^{3+}$ and a gain of $\text{Ru}(\text{bipy})_3^{2+}$, with no other infra-red active products being observed, see fig. 7. Initially, it was thought that this process was the Pt-O catalysed oxidation of water by $\text{Ru}(\text{bipy})_3^{3+}$: it has been known for many years that the reaction:



is catalysed by a wide range of transition-metal oxides[38][39], and at the potential of 1.2 V vs SSCE the surface of Pt is expected to be covered by an oxide layer. However, similar excess charges were subsequently found for films on basal-plane graphite, and UV spectrophotometry was then employed to carry out a more detailed kinetic study. Fig. 8(a) shows the time evolution of the absorbance of the 676 nm band of $\text{Ru}(\text{Bipy})_3^{3+}$ formed in solution by addition of a stoichiometric quantity of $\text{K}_2\text{S}_2\text{O}_8$ to a 2.5 mM solution of $\text{Ru}(\text{Bipy})_3^{2+}$ buffered to pH 2, and irradiated with sunlight until the colour change to the green $\text{Ru}(\text{Bipy})_3^{3+}$ was complete. Line (i) shows a the very slow reduction of $\text{Ru}(\text{Bipy})_3^{3+}$ under normal circumstances in aqueous solution; line (ii) shows the effect of adding $5\text{ }\mu\text{L}$ of 2% Nafion solution to form a dispersed floc; line

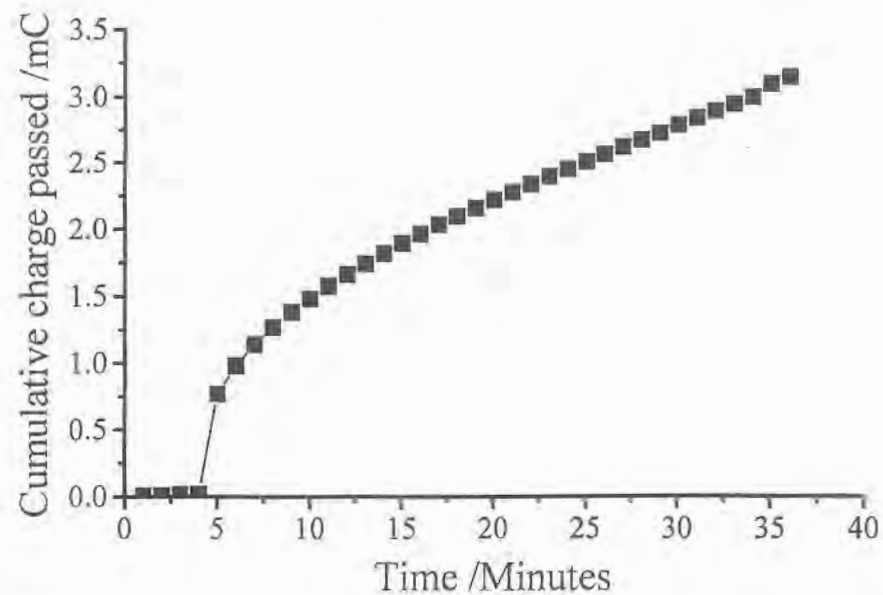
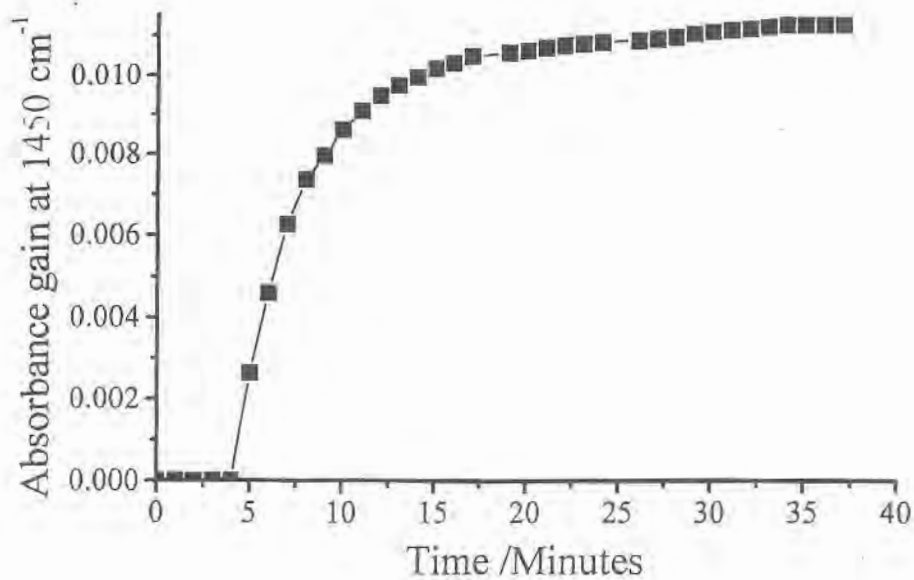


Fig. 6 (a) The intensity of the 1450 cm⁻¹ gain feature observed during an experiment in which the potential of a 4 mM Ru(bipy)₃²⁺ Type (I) film on a Pt electrode in pH 2 0.2M K₂SO₄ was stepped from 0.8V to 1.2V in a single step, at t = 4 minutes, and spectra (8 cm⁻¹ resolution, 100 co-added and averaged scans, 35 s per scan set) collected as a function of time (b) The charge passed during the oxidation of the Type (I) film in fig 7 as a function of time.

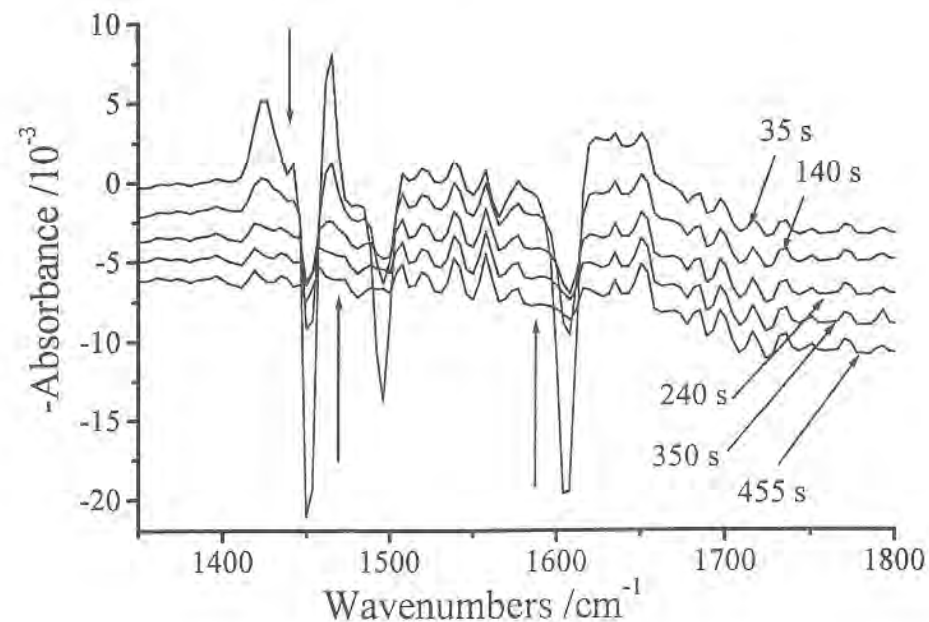
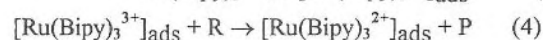
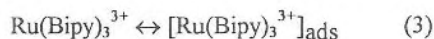


Fig. 7 *In-situ* FTIR Spectra, (8 cm⁻¹ resolution, 100 co-added and averaged scans), of a type (I) film collected after the film was stepped to 1.2V, held until the IR response was constant, and then switched to open circuit. The spectra were collected as a function of time, as shown on the figure, and all normalised to the reference spectrum taken at 0.7V before the potential step. All the features decrease in intensity with time, as shown by the arrows.

(a)

(b)

(iii) the effect of adding 5 μL of an equal mixture (by volume) of ethanol and isopropyl alcohol, and line (iv) shows the effects of adding acid to 0.5M H^+ and subsequent addition of the Nafion. The addition of the alcohols clearly enhances the rate of decay of the Ru(III) complex; both lines (i) and (iii) show excellent fits ($R > 0.999$) to first order decay kinetics, with rate constants of $5.0 \pm 0.02 \times 10^{-5} \text{ s}^{-1}$ and $3.3 \pm 0.004 \times 10^{-4} \text{ s}^{-1}$, respectively. The addition of the Nafion increases the rate of reduction of $\text{Ru}(\text{Bipy})_3^{3+}$ still more; furthermore, kinetic investigation of the Nafion plot shows that the initial loss is zeroth order in $\text{Ru}(\text{Bipy})_3^{3+}$, which suggests that the reduction is mediated by adsorption on the floc. The data in fig. 8(a), line (ii), if presented as a first order plot give a rate constant of $c. 10^{-2} \text{ s}^{-1}$, but the fit is very poor. In fact, these data can, in fact, be understood quantitatively on the basis of the reaction scheme:



where R appears to be alcohol or possibly water. This second reaction is slow, and has the reaction rate $v = -dc/dt = k\theta^n$, where c is the concentration of $\text{Ru}(\text{Bipy})_3^{3+}$ and θ its coverage on the surface of the floc. If a Langmuir Isotherm is assumed for adsorption of the complex, and n is set at 1:

$$-dc/dt = k\theta \quad (5)$$

$$-dc/dt = kKc/(1 + Kc) \quad (6)$$

where K is the Langmuir adsorption equilibrium constant.

$$-dt/dc = (1/kKc) + 1/k \quad (7)$$

$$-dt/dc = (1/k) \cdot [(1/Kc) + 1] \quad (8)$$

Integrating (8), setting $c = c_0$ at $t = 0$, and re-arranging gives:

$$[(1/K) \cdot \ln c + c] = -kt - [(1/K) \cdot \ln c_0 + c_0] \quad (9)$$

The concentration c of the $\text{Ru}(\text{Bipy})_3^{3+}$ was calculated from the extinction coefficient at 676 nm, which was measured and found to be $120 \pm 10 \text{ mol}^{-1} \text{ dm}^3 \text{ cm}^{-1}$. K was obtained by a process of iteration, with a value of $c. 1100 \pm 100 \text{ mol}^{-1} \text{ dm}^3$ giving a highly linear plot, as can be seen in fig. 8(b). Finally, it is noteworthy that the rate of reduction of $\text{Ru}(\text{Bipy})_3^{3+}$ in solution does not depend on pH, see fig. 8(a) line (iv), but catalysis by Nafion does appear to be inhibited at high proton concentrations, possibly because protonation of the sulphonate groups of the Nafion becomes significant at $\sim 0.5 \text{ M H}^+$, preventing ionosorption of $\text{Ru}(\text{Bipy})_3^{3+}$. The OCV IR response shown in fig. 7 can also be fitted to the same model; fig. 9 shows the corresponding plot to that in fig. 8(b) for the absorbance of the 1450 cm^{-1} $\text{Ru}(\text{Bipy})_3^{3+}$ band in fig. 7.

The work showed quite clearly that the 'steady state' current observed after the oxidation of $\text{Ru}(\text{Bipy})_3^{3+}$ in Nafion is due to the fact that Nafion catalyses the reduction of the Ru(III) complex, the concomitant oxidation reaction being either conversion of residual alcohols in the film to aldehydes, or (less probably) evolution of oxygen from water. In addition to the aspects of the work discussed above, we were able to show [11] that charge conduction in the system is predominantly *via* diffusion, with electrons shuttled between the electrochemically easily accessible pore region of the

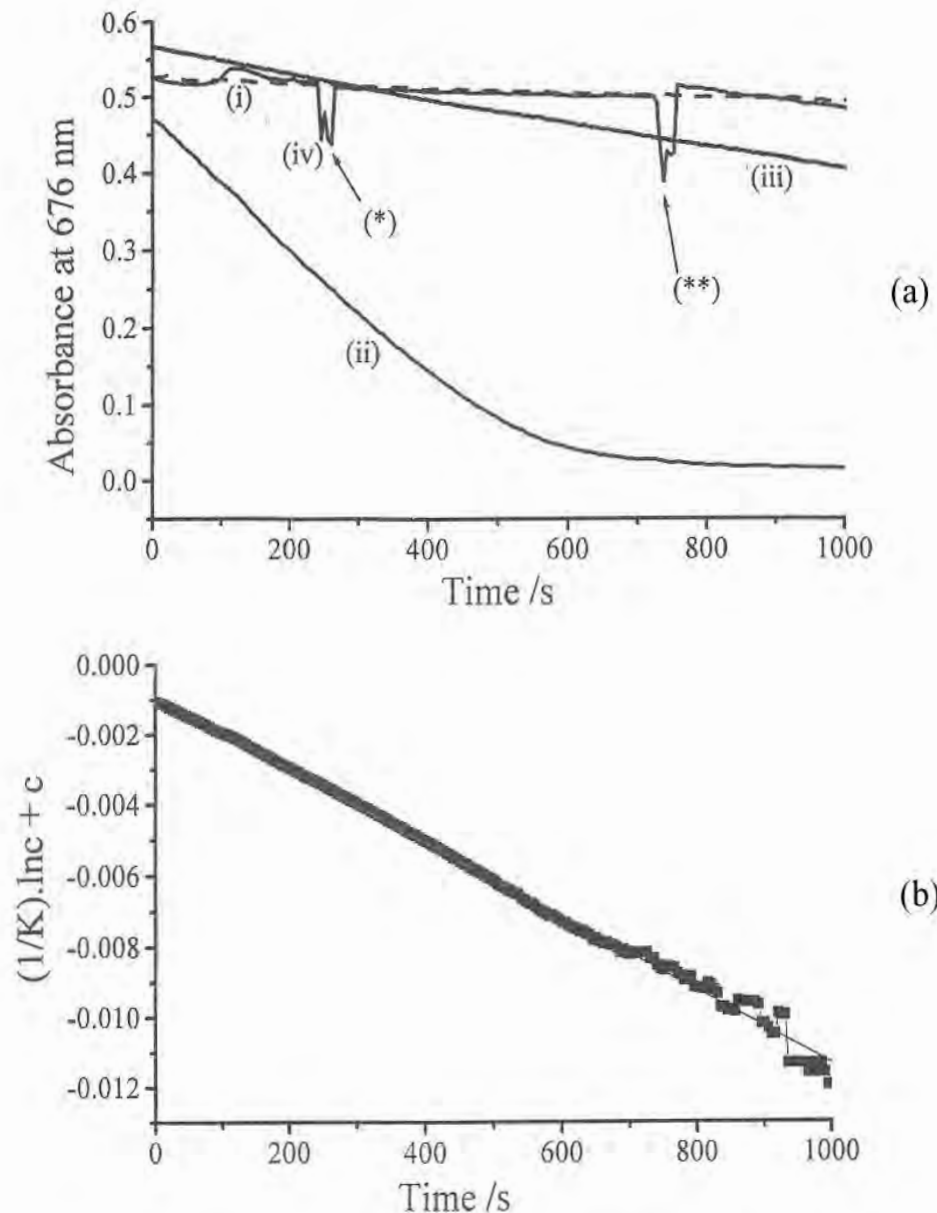


Fig. 8 (a) Absorbance at 676 nm monitored (i) [dashed line] after the oxidation of 2.5 mM $\text{Ru}(\text{bipy})_3^{2+}$ by 1.25 mM $\text{K}_2\text{S}_2\text{O}_8$ in pH 2 0.2M K_2SO_4 in a 1 cm-pathlength cell, (solution volume 4 cm^3). The solution was irradiated immediately after the addition of the $\text{K}_2\text{S}_2\text{O}_8$ using a tungsten-halogen lamp (Osram), before placing the cell in the spectrometer. (ii) As for (i), except after the addition of 5 μL of 2% Nafion solution and thorough mixing. (iii) As for (i) except after the addition of 5 μL of an equal mixture (by volume) of ethanol and isopropyl alcohol and mixing. (iv) As for (i) except (*) 100 μL of conc. H_2SO_4 were added, followed by (**) 5 μL of 2% Nafion solution. (b) The data in (a), curve (ii), modelled as a first-order decay process at the Nafion surface, (see text for details).

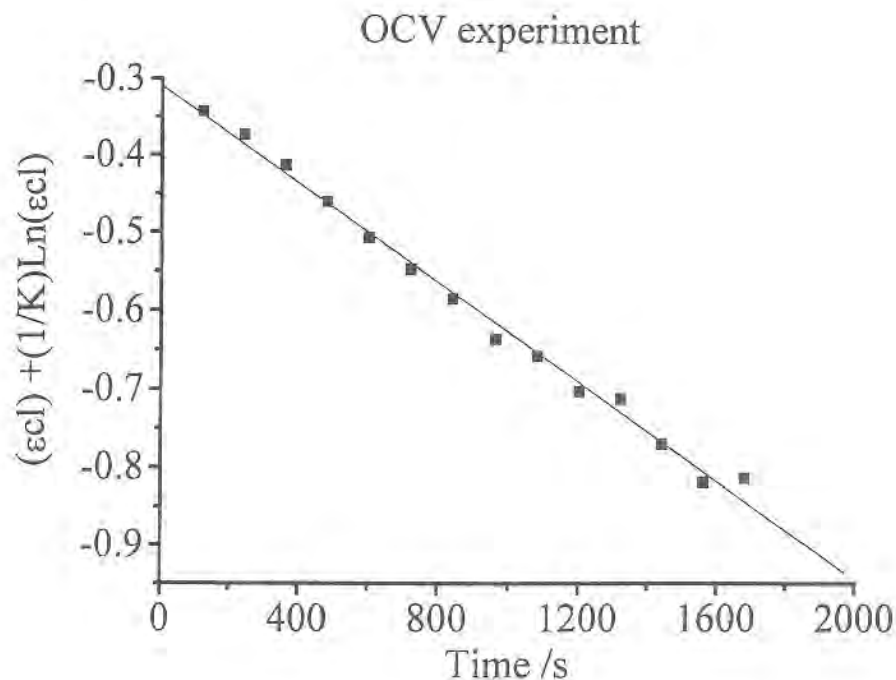


Fig. 9 The intensity of the 1450 cm^{-1} $\text{Ru}(\text{Bipy})_3^{3+}$ feature in fig. 7 modelled as a first-order decay process at the Nafion surface, (see text for details).

film and the backbone hydrophobic region by 'messenger' $\text{Ru}(\text{Bipy})_3^{2+}$ species present in the interfacial region.

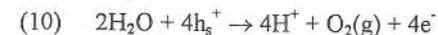
3.3 The oxidation of methanol at irradiated thermal TiO_2 films as a function of temperature

Figure 10 shows cyclic voltammograms of the thermal film electrode immersed in 1M methanol/0.1M NaClO_4 in the dark and under irradiation at $50\text{ }^\circ\text{C}$; the enhanced currents observed on irradiation at potentials $< c. 0.5\text{ V}$ are associated with the oxidation reduction process, and have been attributed to the formation of peroxytitanates[40]. The cyclic voltammograms observed with and without methanol at $10\text{ }^\circ\text{C}$ and $50\text{ }^\circ\text{C}$ were essentially identical, and hence fig. 10 may be taken as representative for all these conditions. The fact that methanol had no effect upon the cyclic voltammetry under irradiation suggests the possibility that hole capture at the interface, whether by methanol or water, is not rate limiting. Another possibility, not necessarily at odds with this, is that the current is dominated by a single hole capture event that leads to different products depending upon electrolyte composition.

3.3.1 Experiments at $10\text{ }^\circ\text{C}$ and $50\text{ }^\circ\text{C}$ in the absence of methanol.

Figure 11 shows FTIR spectra taken at $+1.2\text{ V}$ vs Ag/AgCl and at $10\text{ }^\circ\text{C}$ and $50\text{ }^\circ\text{C}$ under irradiation. The spectra were collected at the end of experiments in which the potential was stepped up in 100 mV increments from -0.1 V , spectra (100 co-added and averaged scans at 8 cm^{-1} resolution) collected at each step and normalised to the reference spectrum taken at -0.1 V at the same temperature. The corresponding spectra collected in the dark were essentially featureless, showing only very weak, ($< 2 \times 10^{-4}$ absorbance), gains of solution ('bulk') ClO_4^- near 1108 cm^{-1} [15][17][35]. This correlates with the small and near constant anodic current of fig. 10 (dark) which is probably due to the slow depopulation of surface states. Under irradiation, both the spectra in fig. 11 show marked loss features, which may be unambiguously attributed to the physical loss of electrolyte[15][17][18][41] caused by the evolution of gaseous O_2 in the thin layer.

The small gains of dissolved CO_2 in fig. 11, (band near 2340 cm^{-1} [37]), are somewhat surprising at first sight, given the absence of any added organic. This has been routinely observed in other studies[15][17][18][41] using both sol-gel- and thermally-fabricated TiO_2 photoanodes, and may be attributed to the release of CO_2 from HCO_3^- in solution and/or adsorbed on the TiO_2 surface owing to the drop in pH occasioned by the oxidation of water at the TiO_2 :



where h_s^+ refers to a photogenerated hole at the electrode surface. It is believed that the first step is:



a process that appears to be extremely fast.

Evidence in support of an overall gain of positive charge in the electrolyte thin layer is provided by the observation of the bulk ClO_4^- gain feature near $c. 1108\text{ cm}^{-1}$ in fig. 11, owing to anion being drawn into the thin layer to provide charge compensation.

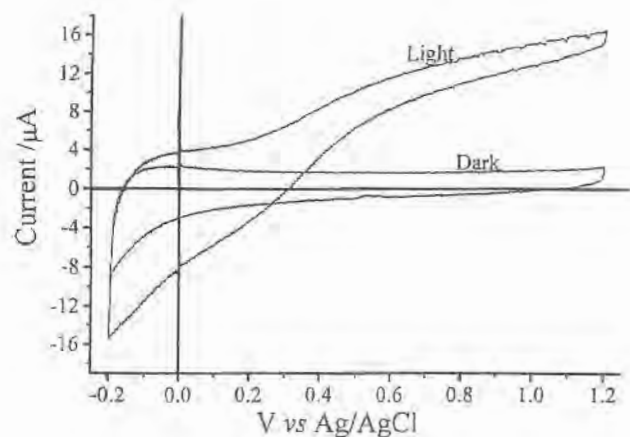


Fig. 10 Cyclic voltammograms of a thermal TiO_2 film electrode, 0.64 cm^2 , immersed in $0.1 \text{ M NaClO}_4/1 \text{ M CH}_3\text{OH}$ at 50°C in the dark, and under irradiation with UV light (150 W Xe lamp) via a 1 m flexible liquid light guide. Scan rate 100 mV s^{-1} .

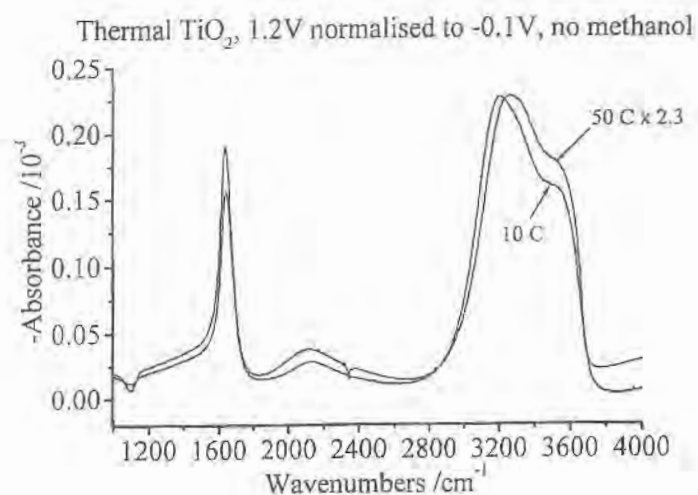


Fig. 11 *In-situ* FTIR Spectra, (8 cm^{-1} resolution, 100 co-added and averaged scans), collected from the electrode in fig. 10 immersed in 0.1 M NaClO_4 and under irradiation at 1.2 V vs Ag/AgCl at 10°C and 50°C . The spectra were each collected at the end of an experiment in which the potential was stepped up from -0.1 V in 100 mV increments, spectra collected at each step and normalised to the reference spectrum taken at -0.1 V at the specified temperature. The spectrum collected at 50°C has been scaled by a factor of 2.3, for clarity.

In essence, the loss features in fig. 11 may be regarded simply as the absorbance spectra of water at the two temperatures. The main features may be assigned as follows[42]: the ν_1 and ν_2 O-H stretches near $c. 3400 \text{ cm}^{-1}$, the ν_3 deformation near 1640 cm^{-1} and a weak combination band[43] near 2100 cm^{-1} , all of which show temperature-dependent frequencies and intensities. This latter 'Association band' is believed to be a combination band of ν_3 and a hindered rotation or 'intermolecular band'[43] which absorbs near 500 cm^{-1} [42]. Closer inspection of fig. 11 shows that: ν_2 increases in frequency from $c. 3200 \text{ cm}^{-1}$ to 3260 cm^{-1} on increasing the temperature from 10°C to 50°C ; the combination band decreases from 2130 cm^{-1} to 2117 cm^{-1} , and ν_3 decreases from 1645 cm^{-1} to $c. 1638 \text{ cm}^{-1}$, in agreement with the literature[42][43].

Figure 12 shows a plot of the area under the O-H stretch bands in fig. 11 as a function of potential; at both temperatures, the cumulative charge passed during the data collection was $c. 2.8 \text{ mC}$. It is clear from the figure that the intensity of the band(s) is significantly lower at 50°C than at 10°C at higher potentials, and apparently reaches a steady value at potentials $> 0.9 \text{ V}$ at 50°C . This could simply be due to a decreased thickness of the thin electrolyte layer in the experiment conducted at 50°C , such that the levelling out represents the complete loss of electrolyte from the thin layer. However, if this were the case, the observation of steadily increasing gain features, such as CO_2 and ClO_4^- , would not be expected in fig. 11. Moreover, a comparison of the single beam spectra taken at -0.1 V in fig. 11 showed that the thin layer thicknesses, estimated from the $2700 \text{ cm}^{-1} - 4200 \text{ cm}^{-1}$ regions of the spectra, are very similar. A rough estimate of the absorbances at $c. 3200 - 3300 \text{ cm}^{-1}$ in the single beam spectra gives values of 0.73 and 0.76, far greater than the absorbance of the loss features at the same frequencies in fig. 11. The expulsion of the water is most likely to be due to the formation of small bubbles of O_2 that have nucleated and grown on the TiO_2 surface. Such bubbles may remain attached to the TiO_2 surface or may become detached, in which case they will migrate out of the thin layer. At 10°C the rate of detachment is clearly small, since there is a steady, and approximately linear, increase in water loss with charge passed. The establishment of a steady state at 50°C , by contrast, suggests a significantly higher detachment rate such that, above 0.9 V , the rate of bubble formation and bubble detachment become equal.

One notable feature of fig. 12 is that the onset potential at which significant current passes is noticeably more anodic than that in fig. 10. The apparent delay observed in fig. 12 before appreciable loss of water occurs, which is reflected in the plots of cumulative charge measured during the FTIR experiments vs. potential, has been observed in earlier work[15], and has been explained in terms of a shift in pH in the thin layer due to water oxidation. The flatband potential, and hence photocurrent onset potential, are pH dependent, shifting up as the pH decreases by 59 mV per pH[44]. If it assumed that all the charge passed until the onset of appreciable Faradaic reaction at 0.5 V , 0.5 mC , resulted in the oxidation of water, this would correspond to a final pH of 1.8 in the thin layer. The shift is dynamic, and hence the flatband potential moves steadily more positive.

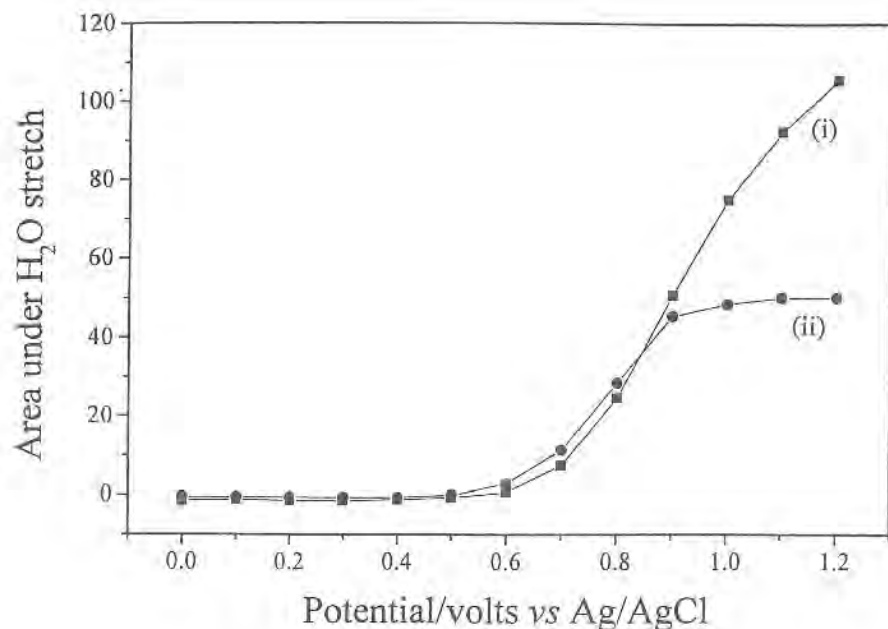


Fig. 12 Plots of the area under the $c. 3500 \text{ cm}^{-1}$ water bands from the experiments in fig. 11 taken as a function of potential; (i) $10 \text{ }^\circ\text{C}$ and (ii) $50 \text{ }^\circ\text{C}$.

3.3.2 Experiments at $10 \text{ }^\circ\text{C}$ and $50 \text{ }^\circ\text{C}$ in the presence of methanol

Addition of 1M methanol to the electrolyte caused no change in the cyclic voltammograms, but marked changes in the *in-situ* FTIR spectra, both in the dark and under irradiation. The data taken in the dark will not be discussed for reasons of space, but is dealt with in detail in ref. [27].

3.3.2.1 Experiments at $10 \text{ }^\circ\text{C}$ under irradiation

Figure 13(a) shows spectra taken during a repeat of the experiment depicted in fig. 11, but in the presence of methanol, and fig. 13(b) plots of the intensities of the various features in fig 13(a) as a function of potential; one immediately apparent observation is that there is no marked water loss, suggesting that the formation of oxygen bubbles is not taking place, and implying that the active $\cdot\text{OH}$ species produced in reaction (10) above have been intercepted.

At potentials below $c. 0.5 \text{ V}$, the spectra of fig. 13(a) are dominated by the gain of water features at 1660 cm^{-1} and 3100 cm^{-1} . These features were observed to increase steadily as the potential was increased in the dark experiment, and were attributed[27] to a form of bulk water associated with a change in ionic strength. In the dark, the 1660 and 3100 cm^{-1} bands were accompanied by gains of solution methanol, band near 1015 cm^{-1} , and adsorbed ClO_4^- , and hence it was postulated that the water bands were the result of a change in ionic strength caused by the adsorption of the anion and concomitant desorption of methanol as the ionic strength increased. At 0.2 V , after passing a charge of $\sim 100 \mu\text{C}$, there is a marked relationship to the spectra observed in the dark experiment, save that the changes seen in the water structure are an order of magnitude smaller, and there is a gain of solution ClO_4^- rather than ionosorbed ClO_4^- . There is also no gain of a peak at 1015 cm^{-1} . All this suggests that adsorbed methanol is probably being oxidised, even at these low potentials in the light, rather than desorbed, and there is evidence for CO_2 formation at potentials above 0.2 V , (see fig. 13(a)). Clearly far less methanol is being lost overall from the surface at 0.2 V in the light than at 1.2 V in the dark, and this accounts for the much smaller change in water structure; the solution ClO_4^- seen is probably material diffusing into the optical path from the bulk solution outside the thin layer to compensate the charge passed.

It is clear from figs. 13(a) & (b) that, not only is the formation of bubbles suppressed in the presence of methanol, but that CO_2 is not evolved until potentials $> 0.2 \text{ V}$. The CO_2 feature is weak, however, and this low intensity strongly suggests that it is not the main product of the Faradaic reaction. This postulate is backed up by some simple calculations: the water absorbance at 3500 cm^{-1} in the single beam reference spectrum taken during the experiment depicted in fig. 13(a) is $c. 0.73$; using an extinction coefficient appropriate for $10 \text{ }^\circ\text{C}$ of $55 \text{ mol}^{-1} \text{ dm}^3 \text{ cm}^{-1}$ [42] gives a thin layer thickness

¹ The ClO_4^- feature observed in the dark at $10 \text{ }^\circ\text{C}$ is narrower than the corresponding band observed in fig. 11, which were attributed to fully solvated anions. (Width at Half Peak Height = 56 cm^{-1} *cf.* 67 cm^{-1} in fig. 11), and slightly higher in frequency.

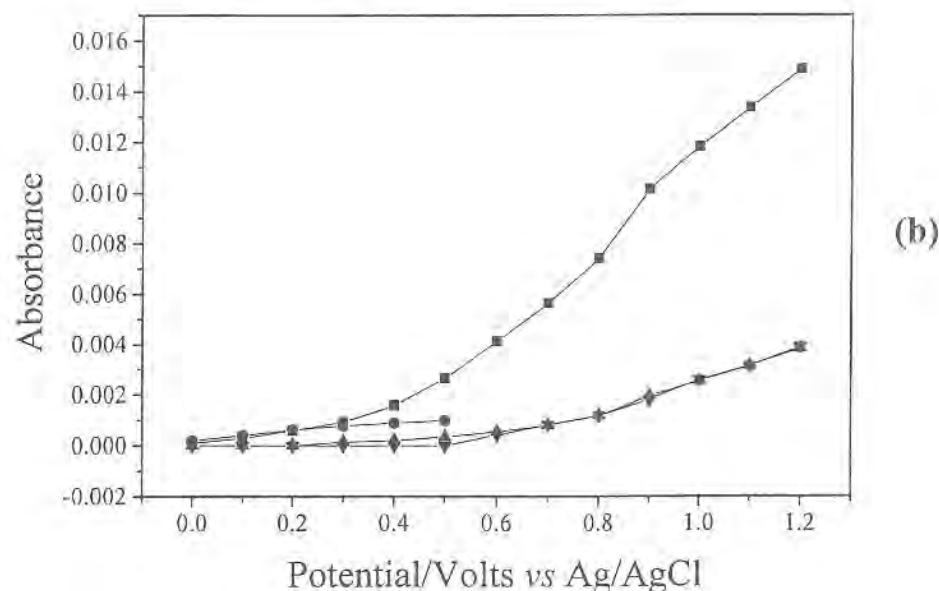
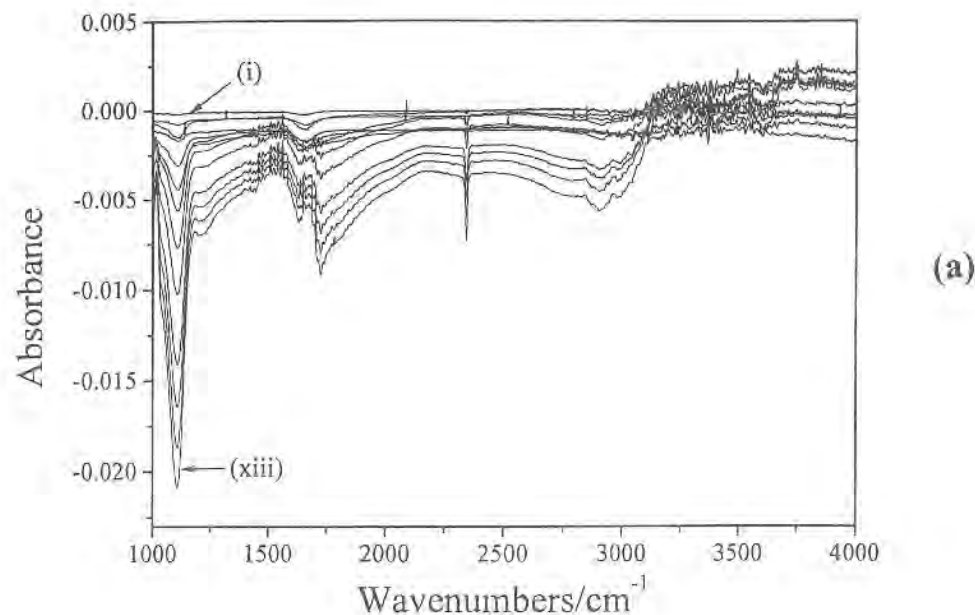


Fig. 13 (a) A repeat of the experiment at 10 °C shown in fig. 11, except in the presence of 1 M MeOH; (i) 0 V to (xiii) 1.2V. (b) Plots of the intensities of the various features in fig. 9(a) as a function of potential. ■ 1108 cm⁻¹; ● 1660 cm⁻¹; ▲ CO₂ and ▼ 1015 cm⁻¹.

of *c.* 1.2 μm. The CO₂ absorbance of *c.* 4×10^{-4} hence corresponds to *c.* 10^{-9} moles, using an extinction coefficient of 1200 mol⁻¹ dm³ cm⁻¹[45], and assuming 10^{15} atoms cm⁻², this corresponds to the oxidation of a monolayer of adsorbed methanol. Such a process would require only *c.* 580 μC, < 20% of the charge actually passed, suggesting that there is a, as yet unidentified, primary oxidation product. At potentials > 0.5V, there is also the clear loss of the solution methanol band at 1015 cm⁻¹ (see fig. 13(b)) which is apparently accompanied by the gain of two features near 2900 cm⁻¹. In fact, closer inspection of fig. 13(a) reveals a shoulder towards the low energy side of the ClO₄⁻ gain feature suggesting, perhaps, the gain of a C-O stretch. This shoulder tracks the gain of the two features near 2900 cm⁻¹. The possible products of the oxidation of methanol are somewhat limited; in fact, it is known that [•]OH radicals react with excess methanol to give formaldehyde as the principal stable product[46]; a reaction that was employed by Sun and Bolton[47] to determine the quantum yield for [•]OH formation at irradiated Anatase suspensions. In aqueous solution, formaldehyde exists as the hydrate, CH₂(OH)₂[48], and a spectrum of a 1M solution of formaldehyde in pH 2.5² NaClO₄ is shown in fig. 14. Not only is there a strong, low energy feature due to the C-O stretch of the formaldehyde hydrate, but the two features observed near 2900 cm⁻¹ in fig. 13(a) are also present, lending strong support to the postulate that formaldehyde is the dominant product. Assuming a 2-electron oxidation, the residual charge passed after allowing for the oxidation of the adsorbed methanol would result in the formation of *c.* 0.18M formaldehyde in the thin layer.

At potentials above 0.4V there is a large increase in the perchlorate absorption, accompanied by the appearance of a broad absorption between 1500 cm⁻¹ and *c.* 3200 cm⁻¹, which may be attributed to H₃O⁺[49]. The appearance of this absorption distorts the region around the 1660 cm⁻¹ water absorption, making the intensity of the latter difficult to track; however, it does appear that the water absorptions decline at potentials > 0.5V. The potential dependence of the ClO₄⁻ gain feature clearly shows that the oxidation of adsorbed methanol to CO₂ is not the only Faradaic process generating positive charge taking place, since appreciable Faradaic charge does not pass until potentials > 0.5V, yet the perchlorate feature increases in intensity at all potentials > -0.1V, (see fig. 13(b)).

To summarise, at 10 °C in the dark, TiO₂ chemisorbs methanol at low potentials; as the potential is increased, the methanol is desorbed and replaced by chemisorbed perchlorate (and associated cations) from solution, giving rise to characteristic IR changes, including some unusual water-like features. In the light, at potentials above ~ 0.2 V, the chemisorbed methanol is steadily oxidised, possibly to CO₂, but the main oxidation process converts solution-phase methanol to hydrated formaldehyde, with concomitant diffusion of ClO₄⁻ from the bulk electrolyte into the thin layer.

² To mimic the conditions extant after proton formation in the thin layer.

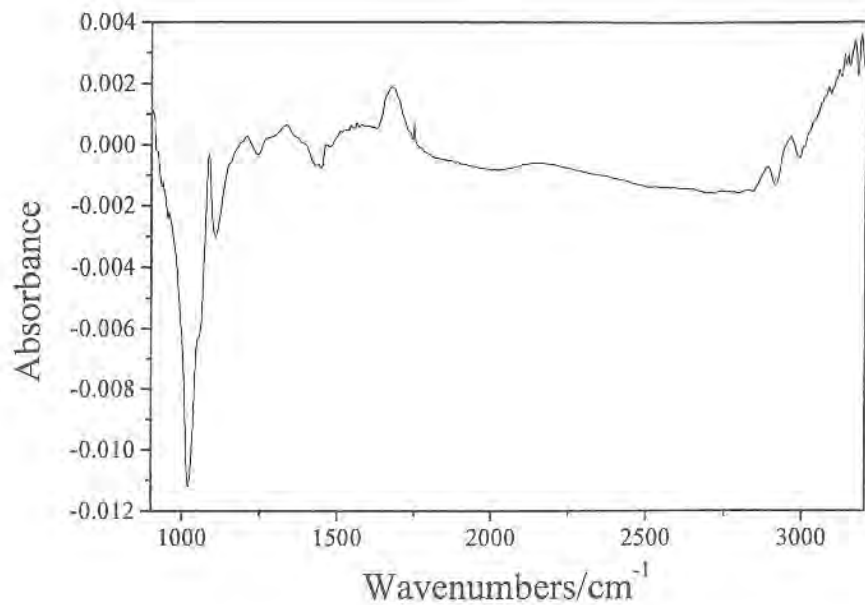


Fig. 14 Reflectance spectrum of 1M formaldehyde in pH 2.5 HCl/0.1M NaClO₄. The spectrum was obtained by flushing the electrolyte containing the formaldehyde into the *in-situ* FTIR cell, taking spectra (8 cm⁻¹ resolution, 100 scans) as a function of time and normalising to the reference spectrum taken of the electrolyte only

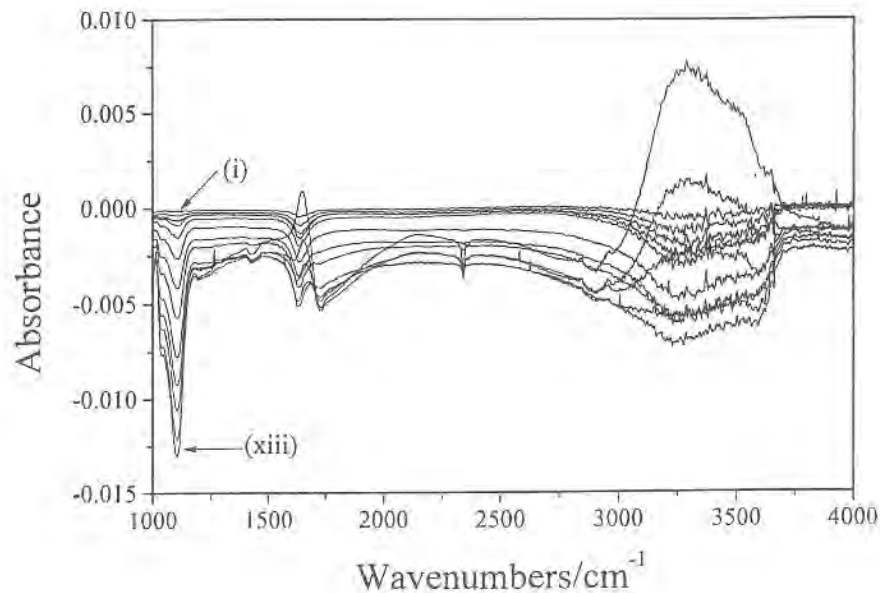
3.3.2.3 Experiments at 50 °C under irradiation

Fig. 15(a) shows a repeat of the experiment in fig. 13(a), only carried out at 50 °C, and fig 15(b) plots of the intensities of the main features observed in fig 15(a) as a function of potential. There are now clear gains of 'bulk' ClO₄⁻ at 1100 cm⁻¹ and of solution formaldehyde, accompanied by the loss of the solution methanol at 1015 cm⁻¹. There is also clear evidence of gain of H₃O⁺, and of CO₂. However, closer investigation reveals additional gain features near 1300 cm⁻¹, 1440 cm⁻¹ and 1720 cm⁻¹ that clearly track the loss of the methanol. These features can be attributed to methyl formate[50], with the latter also possibly arising from formic acid. At lower potentials, similar water-like features are seen, again arising from changes in ionic strength.

It is noteworthy that the rate of loss of the solution methanol peak at 1015 cm⁻¹ is identical to that observed at 10°C, and this strongly suggests that not only is there a common rate-limiting step for photo-oxidation at the two temperatures, but that this step has an extremely low activation energy. In fact, the rate-limiting process must be the rate of photo-generation of holes, or, more accurately, the rate of their arrival at the interface, and each hole must, eventually, be captured by a methanol molecule, either directly, or through mediation by [•]OH. However, there are marked differences in the amount of CO₂ generated at the two temperatures in the light; at 10°C, far more CO₂ is observed, suggesting that this latter probably arises from direct hole capture by chemisorbed methanol. In agreement with this, is the fact that the production of CO₂ at 50°C is about three times lower than at 10°C, corresponding to the factor of three seen in the water structure size in the two spectra *in the dark*, and suggesting a reduction in coverage by methanol of a factor of three as the temperature is raised from 10 to 50°C.

Above 0.8 V, the spectra of fig. 15(a) clearly show the loss of bulk water features, indicating the onset of oxygen bubble formation, which may reflect the enhanced surface mobility of [•]OH_{ads} at higher temperatures. The concentration of these species will rise with potential, their mobility is likely to be enhanced by the lower methanol coverage, and mobility will be a key factor in determining whether formation of O₂ or attack on methanol is favoured. It is also noteworthy that at 50°C, both formaldehyde *and* formic acid are formed as partial oxidation products. Both products appear to originate from solution methanol rather than adsorbed methanol, but formate will require additional holes or [•]OH_{ads} species at the interface; the more mobile the latter, the more probable it becomes that higher oxidation products will form, even for non-chemisorbed species.

At first glance, the electrochemistry and photo-electrochemistry of TiO₂ in the presence of methanol appears to be all but identical at 10°C and 50°C. However, *in situ* FTIR spectroscopy shows clearly that there are substantial differences. These differences are associated, at least in part, with a reduction in methanol coverage at the higher temperature, and this reduction leads to quite different distributions of products. At the lower temperature, where methanol coverage is high, the main routes are to CO₂ and to formaldehyde. It would appear at least plausible that chemisorbed



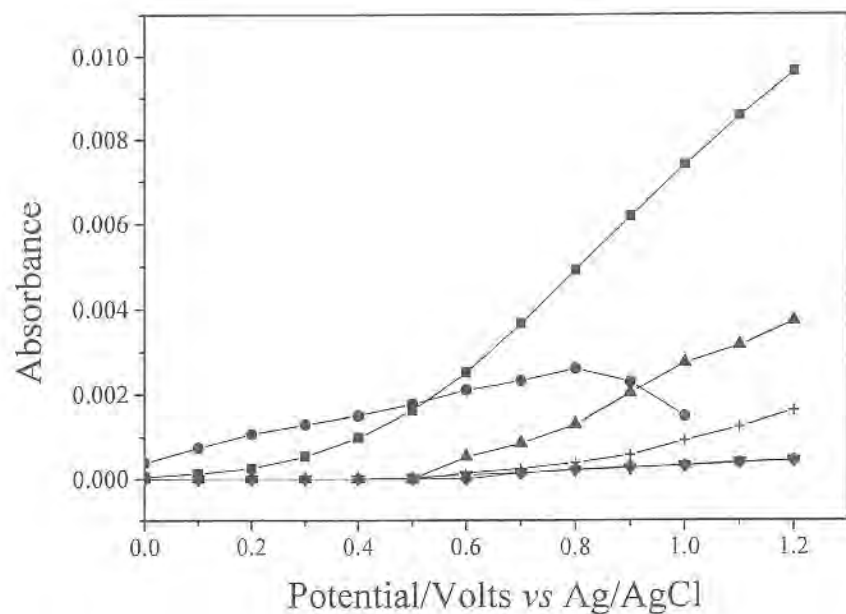
(a)

methanol can be oxidised to CO_2 but that solution methanol is oxidised by a process involving $^{\circ}\text{OH}_{\text{ads}}$ and that the resultant formaldehyde can diffuse away from the surface before further attack. At higher temperatures, methanol coverage is lower, as is CO_2 formation, but the enhanced mobility of the $^{\circ}\text{OH}_{\text{ads}}$ species allows further attack on formaldehyde before it can diffuse away completely.

A major interest in this study has been the remarkable way in which small changes in ionic strength can be amplified by the configuration of the spectro-electrochemical cell to give substantial spectral features. These features are far too large to be associated with any simple product formation, particularly given the small charges passed in the dark, and clearly depend on the amplification associated with solvation throughout the thin layer. We believe that our assignment of these features to changes in ionic strength are strongly backed up by the diffusion experiments carried out, and by other observations in the literature, and that the results of *in situ* FTIR experiments carried out in aqueous solution need always to be examined carefully for effects of this sort.

4. Acknowledgements

I should like to thank the organisers of the joint Xth meeting of the Portuguese Electrochemical Society/Vth Iberian Meeting of Electrochemistry for inviting me to present this work as a Plenary Lecture. I would also like to acknowledge my collaborators on the various research projects described in this work: Professor A. Hamnett, Dr. I. Blackham and Ms. J. Eameaim, as well as the EPSRC and the Department of Chemistry, Newcastle University, for funding for the FTIR spectrometers and electrochemical systems.



(b)

Fig. 15 (a) A repeat of the experiment in fig. 13(a) carried out with the TiO_2 electrode under irradiation (at 50°C), (i) 0 V to (xiii) 1.2V. (b) Plots of the intensities of the various features in fig. 12(a) as a function of potential. \blacksquare 1108 cm^{-1} ; \bullet 1638 cm^{-1} ; \blacktriangle 1015 cm^{-1} ; \blacktriangledown 1440 cm^{-1} ; \blacklozenge 1720 cm^{-1} and $+$ CO_2 .

5. References

1. P.A. Christensen and A. Hamnett, *Comprehensive Chemical Kinetics* 29 (1989) 1.
2. P. A. Christensen and A. Hamnett, "Techniques and Methods in Electrochemistry", Blackie, Chapman and Hall, London, 1994.
3. P.A. Christensen, A. Hamnett and I. Blackham, *J. Electroanal. Chem.* 318 (1991) 407.
4. M. Yagi, K. T. Mitsumoto and M. Kaneko, *J. Electroanal. Chem.*, 437 (1997) 219.
5. J. Zhang, M. Yagi and M. Kaneko, *J. Electroanal. Chem.*, 437 (1997) 219.
6. H. L. Yeager and A. Steck, *J. Electrochem. Soc.*, 128 (1981) 1880.
7. (a) C. R. Martin, I. Rubenstein and A. J. Bard, *J. Amer. Chem. Soc.*, 104 (1982) 4817; (b) H.S. White, J. Leddy and A.J. Bard, *J. Amer. Chem. Soc.* 104 (1982) 4811.
8. (a) D. A. Buttry and F. C. Anson, *J. Amer. Chem. Soc.*, 104 (1982) 4824, (b) D. A. Buttry and F. C. Anson, 105 (1983) 685.
9. I. Rubenstein, *J. Electroanal. Chem.*, 188 (1985) 227.
10. W. J. Vining and T. J. Meyer, *J. Electroanal. Chem.*, 237 (1987) 191.
11. P. A. Christensen, J. Eameaim and A. Hamnett, in preparation.
12. K. A. Ataka and M. Osawa, Joint ISE and Electrochemical Society Meeting, Paris, Aug. 31 - Sep. 5, 1997, Extended Abstracts, Abstract 840, p973.
13. B. A. Blajeni, M. A. Habib, I. Taniguchi and J. O'M. Bockris, *JEAC* 157 (1983) 399.
14. L. M. Peter, D. J. Blackwood and S. Pons, *JEAC* 294 (1990) 111.
15. K. E. Shaw, P. A. Christensen and A. Hamnett, *Electrochim. Acta*, 41 (1996) 719 - 728.
16. L. Kavan, P. Krtil and M. Grätzel, *JEAC* 373 (1994) 123.
17. G. M. Walker, Ph.D. Thesis, University of Newcastle, 1998. K. E. Shaw, Ph.D. Thesis, University of Newcastle, 1995.
18. P. A. Christensen, A. Hamnett, R. He, C. R. Howarth and K. E. Shaw, *Trace Metals in the Environment*, 3 (1993) 765.
19. S. A. Walker, P. A. Christensen, K. E. Shaw and G. M. Walker, *J. Electroanal. Chem.*, 393 (1995) 137.
20. I. M. Butterfield, P. A. Christensen, T. P. Curtis and J. Gunlazuardi, *Water Research*, 31 (1997) 675-677.
21. I. M. Butterfield, P. A. Christensen, A. Hamnett, C. R. Howarth, K. E. Shaw, G. M. Walker and S. A. Walker, *J. Applied Electrochem.* 27 (1997) 385.
22. P. A. Christensen, T. P. Curtis, T. A. Egerton and G. M. Walker, in preparation.
23. S. Södergren, A. Hagfeldt, J. Olsson, S. -E. Lindquist, *J. Phys. Chem.*, 98 (1994) 5552.
24. P. A. Christensen and G. M. Walker, "Opportunities for the UK in Solar Detoxification", ETSU S/P4/00249/REP, HMSO, London, 1996 and references therein.
25. A. Sclafani, L. Palmisano and E. Davi, *J. Photochem. Photobiol. A: Chem.*, 56 (1991) 113.
26. A. Mills, R. H. Davies and D. Worsley, *Chem. Soc. Rev.*, 22 (1993) 417, and references therein.
27. P. A. Christensen, J. Eameaim and A. Hamnett, submitted.
28. P. A. Christensen, A. Hamnett, A. R. Hillman, M. J. Swann and S. J. Higgins, *J. Chem. Soc. Far. Trans.*, 88 (1992) 595
29. F. A. Armstrong, H. A. O. Hill and N. J. Walton, *Quart. Rev. Biophys.*, 18 (1985) 261.
30. I. Taniguchi, M. Iseki, H. Yamaguchi and K. Yasukouchi, *J. Electroanal. Chem.*, 186 (1985) 299.
31. D. Elliot, A. Hamnett, O. C. Lettington, H. A. O. Hill and N. J. Walton, *J. Electroanal. Chem.*, 202 (1986) 303.
32. R. G. Greenler, *J. Chem. Phys.*, 44 (1966) 310.
33. C. H. Kline Jr. and J. Turkevich, *J. Chem. Phys.*, 12 (1944) 300.
34. K. M. Omberg, J. R. Schoonover, J. A. Treadway, R. M. Leasure, R. B. Dyer and T. J. Meyer, *J. Am. Chem. Soc.*, 119 (1997) 7013.
35. G. Socrates, "Infrared Characteristic Group Frequencies", John Wiley and Sons, Chichester, 1980.
36. P. L. Mallick, G. D. Danzer, D. P. Strommen and J. R. Kincaid, *J. Phys. Chem.*, 92 (1988) 5628.
37. (a) P.A. Christensen, A. Hamnett and S.A. Weeks, *J. Electroanal. Chem.* 250 (1988) 127; (b) G.R. Mundy, R.J. Potter, P.A. Christensen and A. Hamnett, *J. Electroanal. Chem.* 279 (1990) 257.
38. A. Harriman, G. Porter and P. Walters, *J. Chem. Soc. Far. Trans. 2*, 77 (1981) 2373.
39. A. Harriman, I. J. Pickering, J. M. Thomas and P. A. Christensen, *J. Chem. Soc. Far. Trans. 1*, 84 (1988) 2795.
40. J. Augustynski, *Electrochim. Acta*, 38 (1993) 43.
41. P. A. Christensen, A. Hamnett, R. He, C. R. Howarth and K. E. Shaw, "Electrochemistry and Clean Energy", Ed. J. G.
42. J. J. Fox and A. E. Martin, *Proc. Roy. Soc. (London)*, A174 (1940) 234.
43. D. A. Draegert, N. W. B. Stone, B. Curnutte and D. Williams, *J. Opt. Soc. Am.*, 56 (1966) 64.
44. H. O. Finklea, in "Semiconductor Electrodes", Ed. H. O. Finklea, Ch. 2, Elsevier, New York, 1988.
45. Paul A. Christensen, Andrew Hamnett, Simon J. Higgins and John A. Timney, *J. Electroanal. Chem.*, 395 (1995) 195 - 209.
46. F.-D. Asmus, H. Mockel and A. Henglein, *J. Phys. Chem.*, 83 (1979) 1218.
47. L. Sun and J. R. Bolton, *J. Phys. Chem.*, 100 (1996) 4127.
48. J. D. Roberts and M. C. Caserio, "Basic Principles of Organic Chemistry", W. A. Benjamin, Inc., New York, 1964 p330.
49. P.A. Christensen and A. Hamnett, *J. Electroanal. Chem.*, 260 (1989) 347.
50. T. Iwasita, F. Nart and W. Vilestich, *Ber. Bunsenges, Phys. Chem.*, 94 (1990)